An Estimation of a Billet Temperature during Reheating Furnace Operation

Yu Jin Jang and Sang Woo Kim

Abstract: Reheating furnace is an essential facility of a rod mill plant where a billet is heated to the required rolling temperature so that it can be milled to produce wire. Although it is very important to obtain information on billet temperatures, it is not feasible during furnace operation. Consequently, a billet temperature profile should be estimated. Moreover, this estimation should be done within an appropriate time interval for an on-line application. In this paper, a billet heat transfer model based on 2D FEM (Finite Element Method) with spatially distributed emission factors is proposed for an on-line billet temperature estimation and also a measurement is carried out for two extremely different furnace operation patterns. Finally, the difference between the model outputs and the measurements is minimized by using a new optimization algorithm named uDEAS (Univariate Dynamic Encoding Algorithm for Searches) with multi-step tuning strategy. The obtained emission factors are applied to a simulation for the data which are not used in the model tuning for validation.

Keywords: Billet temperature estimation, emission factors, FEM, reheating furnace, uDEAS.

1. INTRODUCTION

Wire is produced by sending a billet to a rolling machine at rod mil plant. In this process, the billet is heated in a reheating furnace, which should be heated as closely as possible to the required rolling temperature to be milled without any damage to the roller. Typical reheating furnace has three zones (i.e., preheating, heating, and soaking zones) [1-4,10] and some new reheating furnaces have one more soaking zone. After a billet is charged into a reheating furnace, the billet goes through these zones from inlet to outlet and finally it reaches a target temperature. Although it is a fundamental objective of the reheating furnace to heat up the billet to the target temperature, sometimes, in addition to that objective, it is also necessary to control a transient billet temperature pattern according to the material characteristics to prevent a wire from breaking. For example, a steel cord, which is used as a tire reinforcement material, is made of very thin high-carbon steel wire. In general, a billet with a high carbon content has carbon segregation at center side owing to the difference of cooling speed between the billet surface and center after casting. This carbon segregation is one of the major cause of wire-breaking in wire production process. Fortunately, the effect of the carbon segregation can be minimized by controlling the billet temperature according to the predefined special billet temperature pattern in the furnace. Therefore, it is very important to obtain a correct information of billet temperatures. However, it is not feasible to obtain an information of a billet temperature during reheating furnace operation. Consequently, a billet temperature profile should be estimated. In general, since a combustion control of a reheating furnace is done at every 2 minutes and 90 billets can be heated at the same time in the furnace, the billet temperature estimation should be done as fast as possible. Since a 3D FEM model is inappropriate for billet heat transfer model due to its heavy computation time, a 2D FEM model is adopted in this paper. Temperatures of a billet and ambient furnace gas are measured for two extremely different furnace operation patterns. A 2D FEM heat transfer model of the billet with temperature-dependent specific heat and thermal conductivity is constructed. In this 2D FEM model, a boundary condition is considered as a form of radiative heat transfer using an emission factor. Although only a radiative heat transfer term with an emission factor is considered at the boundary of the billet, the effect of convective heat transfer between the billet and its ambient gas and conductive heat transfer between the billet and skid button are taken into account by controlling the emission factor. Hence, the emission factor used in

Manuscript received April 28, 2006; accepted August 26, 2006. Recommended by Editor Jae Weon Choi.

Yu Jin Jang is with the Faculty of Department of Information & Communication Engineering, Dongguk University, Sukjang-dong, Kyungju 780-714, Korea (e-mail: season@dongguk.ac.kr).

Sang Woo Kim is with the Faculty of Electrical and Computer Engineering Division, POSTECH, Pohang 790-784, Korea (e-mail: swkim@postech.ac.kr).

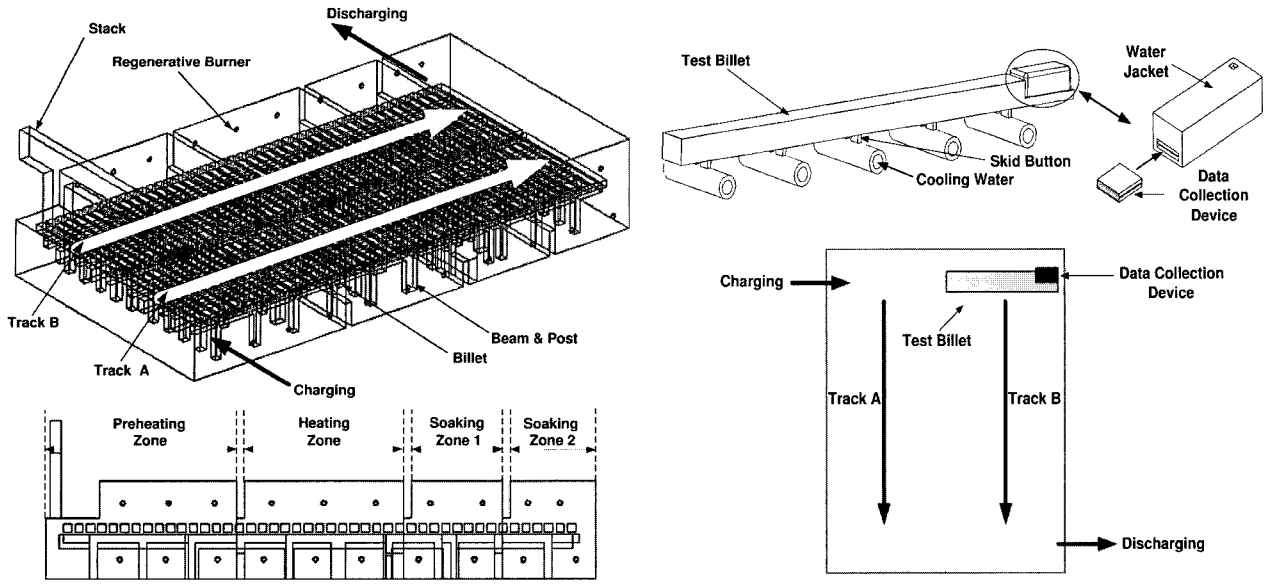

(a) Furnace structure. (b) Experiment setting.

Fig. 1. Furnace structure and experiment setting.

this paper is not a true emission factor but just a tuning parameter. This emission factor (i.e., tuning parameter) is different according to the geometry between billet surface and furnace wall . Hence, this parameter is different according to the billet position in the furnace. Moreover, it is also well known that the emission factor is different according to the billet surface condition. This tuning parameter is also affected by the flow of furnace gas which flows from the soaking zone to the preheating zone owing to the pressure difference. In this paper, it is assumed that this tuning parameter can be represented by the constant between short intervals along the billet moving path. By this assumption, the furnace is divided into 10 parts along the billet moving path and different emission factors are applied on top, bottom and left/right sides of the billet at each part. Subsequently, the difference between the measured billet temperatures and the estimated billet temperatures obtained from the FEM model is minimized by tuning the above emission factors using an optimization algorithm. At this tuning process, uDEAS, which is an effective and easily applicable optimization algorithm, is applied with different cost functions to obtain the optimal emission factors.

2. REHEATING FURNACE AND BILLET TEMPERATURE MEASUREMENT

The reheating furnace at rod mill plant of POSCO (Pohang Iron & Steel Co., Ltd.) consists of four zones (i.e., preheating, heating and soaking zone 1 and 2) and it has two tracks (i.e., billet-moving paths) as shown in Fig. 1(a). The billets move along the track slowly. Also 16, 14, 9, and 6 billets are contained in preheating, heating, soaking zone 1 and 2, respectively, on each track. Therefore, there are 90 billets in the furnace. This furnace is divided into four zones; more clearly than the conventional furnace. Also, the exhaust gas is discharged through the opposite burner by 80%, owing to the operating mechanism of the regenerative burner. Hence, the interference between neighboring zones is reduced significantly compared to the conventional furnace.

Billet temperatures are measured by using a data collection device mounted on a billet as shown in Fig. 1(b). Total of 20 points are selected for measurement by using TC (thermocouples) as shown in Fig. 2. The data collection device is put into a water jacket filled with water. This water jacket is covered with heat protective material to minimize exposure to heat radiation. When the test billet is discharged from the furnace, the data collection device is removed and the stored data are transferred to a PC using a serial cable. This measurement is carried out for the following two extremely different furnace operation patterns:

1) CCR (Cold Charge Rolling) pattern: An operation pattern when the billet with a normal temperature is charged.
2) WCR (Warm Charge Rolling) pattern: An operation pattern when the billet with high initial temperature is charged.

In general, the furnace temperature set value of soaking zones is fixed to satisfy the required rolling temperature of the billet. Therefore, the billet temperature can be controlled by controlling the temperature set value of preheating zone and heating zone. Since the discharging billet temperature is sensitive to the variation of furnace temperature set value of heating zone, the variation range of the

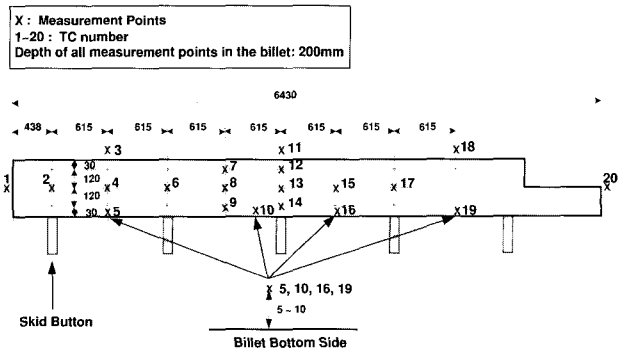

(a) Measurement positions for CCR pattern.

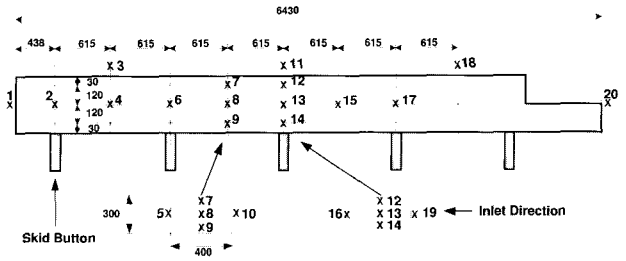

(b) Measurement positions for WCR pattern.

Fig. 2. Measurement positions.

furnace temperature of heating zone is smaller than that of the preheating zone. In practice, the billet temperature pattern is controlled by controlling the furnace temperature of preheating zone. The different furnace temperature set value of preheating zone is the main difference of the above CCR and WCR pattern.

It is observed that the measured temperatures have several characteristics as follows:

1. The ambient temperature of the billet top side along the track is not uniform at the same zone (TC_{11}).
2. The ambient temperature of the billet at a furnace center side is higher than the ambient temperature at furnace wall sides. ($TC_{1,3,11,18,\ and\ 20}$).
3. The ambient temperature of the billet right side (TC_{16}) is higher than the temperature of the billet left side (TC_{19}). The temperature difference between them decreases as the billet is transported through the furnace. Finally, $TC_{11,16,\ and\ 19}$ have similar values at the soaking zones.
4. Also, the billet core temperature (i.e., $TC_{2,4,6,8,13,15,\ and\ 17}$) at the furnace center side is higher than that of the the core temperature at the furnace wall side. For example, $(TC_2 - TC_{17})$ is about $60^{\circ}C$ when the billet is discharged.

Since the part of the billet which is on the skid button is called the skid part, measurement points within the billet can be classified into skid and non-skid parts. The temperatures of the skid and non-skid parts are measured by using TC installed in holes that goes into 10%, 50%, and 90% along the billet thickness direction as shown in Fig. 2 (i.e., $TC_{7,8,\ and\ 9}$ for non-skid part and $TC_{12,13,\ and\ 14}$ for skid part). Since the billet temperature of skid part is lower than that of the non-skid part, the billet temperature of skid part should be greater than the required target temperature. Therefore, only the temperature profiles of skid part will be used for billet heat transfer modeling in the next section.

3. HEAT TRANSFER MODEL

In this section, a temperature-dependent specific heat and thermal conductivity of the test billet are given and then a billet heat transfer model using 2D FEM with spatially distributed emission factors is introduced.

3.1. Material properties

The billet, which is used in the above measurement, consists of the following chief ingredients: (C[%]: 0.326 ~ 0.384, Si[%]: 0.15 ~ 0.30, Mn[%]: 0.70 ~ 0.80, P[%]: $max.$ 0.20, S[%]: $max.$ 0.15). Since it is well known that a specific heat and thermal conductivity of the billet mainly depends on a carbon content, these approximate material properties of the test billet are set as those of carbon content of 0.4% because only the temperature dependent material properties of the carbon content of 0.23%, 0.4% and 0.8% are listed on [5]. The specific heat and thermal conductivity of the material which have carbon content of 0.23% and 0.4% are shown in Fig. 3. Although the thermal conductivity of the material of carbon content of 0.23% and 0.4% shows similar values over the whole billet temperature range, the specific heat shows somewhat different

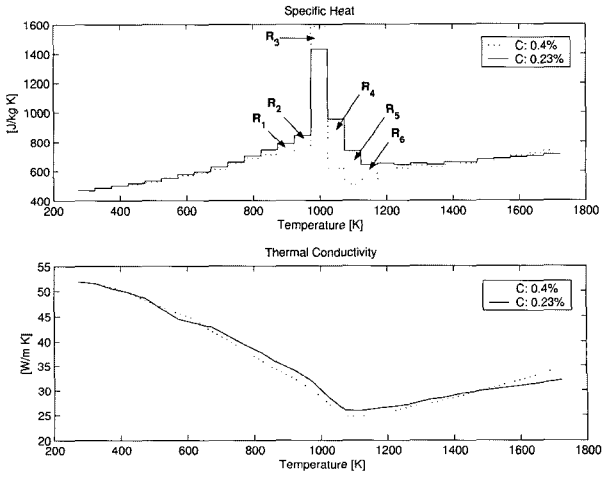

Fig. 3. Material properties.

values on the billet temperature range marked $R_1 \sim R_6$. Since only the conductive heat transfer occurs inside the billet, an incorrect material properties result in an estimation error. Hence, our model will show maximum estimation error near magnetic transformation point (i.e., $R_3 \sim R_4$).

3.2. FEM model

The heat transfer between the billet and the furnace is considerably complex. It consists of the following factors [6]: 1. Radiation from furnace walls, 2. Radiation from gas, 3. Convection from gas, 4. Heat conduction to skid buttons, 5. Heat transfer between the billets. Although a 1D PDE (Partial Differential Equation) model with FEM is adopted to describe the heat transfer of the slab [6,7], a 2D PDE model with FEM is suitable for our problem owing to the shape of the billet as shown in Fig. 1(b). In this paper, only the skid part is used for modeling.

Nomenclature

T	:	billet temperature [K]
t	:	time [sec]
ρ	:	density of the billet = 7800 [kg/m^3]
c	:	specific heat [J/kgK]
k	:	thermal conductivity [W/mK]
x, y	:	coordinate of 2D domain [m]

The heat transfer in the billet is represented as follows [8-10]:

$$\rho c(T)\frac{\partial T}{\partial t} = \frac{\partial}{\partial x}\left(k(T)\frac{\partial T}{\partial x}\right) + \frac{\partial}{\partial y}\left(k(T)\frac{\partial T}{\partial y}\right). \quad (1)$$

The weighted residual form of (1) is

$$\int_{\Omega} W\left[\frac{\partial T}{\partial t} - \frac{\partial}{\partial x}\left(\alpha\frac{\partial T}{\partial x}\right) - \frac{\partial}{\partial y}\left(\alpha\frac{\partial T}{\partial y}\right)\right]d\Omega = 0, \quad (2)$$

where $\alpha = k(T)/\rho c(T)$ and Ω denotes the two-dimensional domain. After applying Green's theorem, (2) can be represented as follows [9]:

$$\int_{\Omega}\left[W\frac{\partial T}{\partial t} + \alpha\left(\frac{\partial W}{\partial x}\frac{\partial T}{\partial x} + \frac{\partial W}{\partial y}\frac{\partial T}{\partial y}\right)\right]d\Omega + \int_{\Gamma_B} W\left(-\alpha\frac{\partial T}{\partial n}\right)d\Gamma = 0, \quad (3)$$

where Γ_B denotes the boundary and $d\Gamma$ denotes the surface element of Γ_B over which the normal gradients are applied. Also n denotes the outward normal unit vector at the boundary Γ. Since the bilinear rectangular element is used as a shape function as shown in Fig. 4(b), T and α are approximated using this shape function as follows:

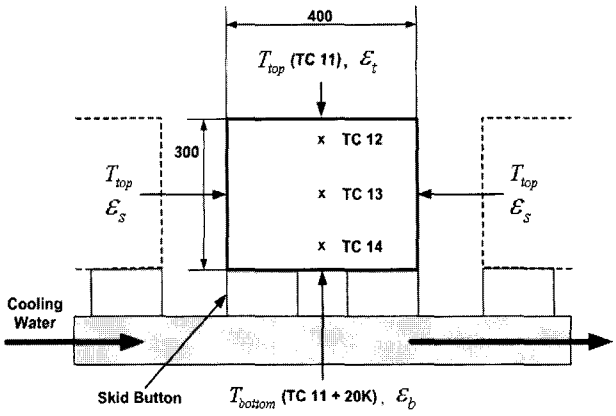

(a) Boundary conditions.

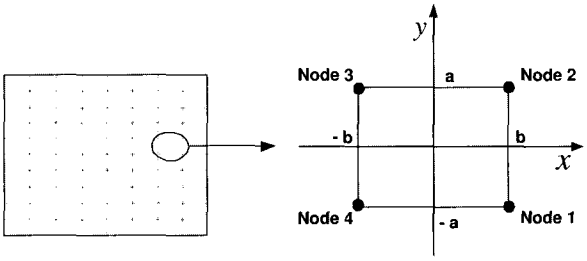

(b) 8×10 mesh generation by using bilinear rectangular element.

Fig. 4. Boundary conditions and mesh generation.

$$T(x,y,t) = \sum_{i=1}^{4} H_i(x,y)T_i(t),$$
$$\alpha(x,y) = \sum_{i=1}^{4} H_i(x,y)\alpha_i, \quad (4)$$

where H_i and α_i are the value of H and α at the node i, respectively, and

$$H_1 = \frac{(b-x)(a-y)}{4ab},\quad H_2 = \frac{(b+x)(a-y)}{4ab},$$
$$H_3 = \frac{(b+x)(a+y)}{4ab},\quad H_4 = \frac{(b-x)(a+y)}{4ab}.$$

The discrete model is obtained by the Galerkin's method with substituting (4) into (3) and setting $W_i = H_i$. A detailed description is given in [8,9].

In this FEM model, 80 bilinear rectangular elements are used and ambient temperatures of the billet are set as shown in Fig. 4(a). The ambient temperature of the billet left and right sides (i.e., a space between billets) is assumed as T_{top}. This can be easily guessed by the observation of the experimental results 3 in the previous section. The furnace temperatures are measured by using sensors attached on top and bottom of the furnace. Since the furnace temperature of the bottom is set higher by 20 K than that of the top, the assumption of the ambient temperature of the billet bottom side, $T_{bottom} = T_{top}$

$+20K$, is appropriate.

Radiative heat transfer at the boundary is represented as follows:

$$-k\frac{\partial T}{\partial n} = 5.67\times10^{-8}(T^4 - T_{amb}^4)\times\varepsilon, \quad (5)$$

where ε is an emission factor. As mentioned in the previous section, the emission factor used in this paper is not an true emission factor but just a tuning parameter (i.e., the heat transfer at the billet boundary is taken into account by controlling the ε in (5)). This emission factor (i.e., tuning parameter) is a function of several factors as mentioned in the previous section. To simplify the problem, it is assumed that this emission factor can be represented by the constant between short intervals along the billet moving path. By this assumption, the furnace is divided into 10 parts along the billet moving path and ε_t, ε_b, and ε_s are applied on top, bottom and left/right sides of the billet, respectively, as shown in Fig. 4(a).

3.3. Controlling billet heat transfer with spatially distributed emission factors

Since it is assumed that the emission factor is a function of position along the track, the furnace is divided into 10 parts, $P_1 \sim P_{10}$, along the track as shown in Fig. 5 and different emission factors are applied on top, bottom and left/right sides of the billet at each part (i.e., $\varepsilon_{t1} \sim \varepsilon_{t10}$ for the billet top side, $\varepsilon_{b1} \sim \varepsilon_{b10}$ for the billet bottom side, and $\varepsilon_{s1} \sim \varepsilon_{s10}$ for the billet left/right side). $T_{ave(CCR)}$ and $T_{ave(WCR)}$ represent average ambient temperature values measured at the top and bottom sides of the furnace for the CCR and WCR patterns, respectively. They have similar patterns except for the preheating zone. If the above emission factors are given, the profiles of the billet temperature can be obtained by using the Crank-Nicolson method [8,9] with the above FEM model and boundary conditions.

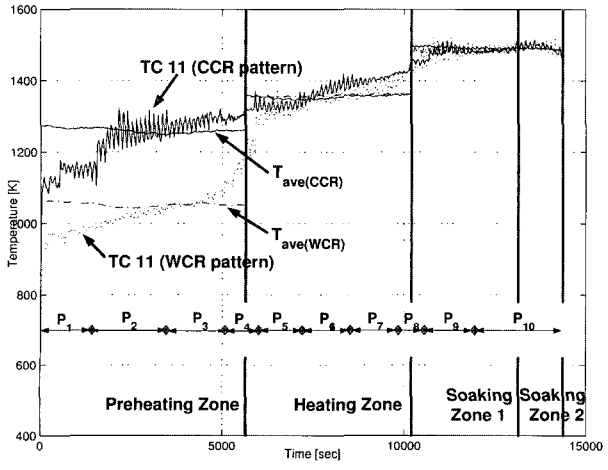

Fig. 5. Division of furnace along the track.

4. ADAPTING THE MODEL TO THE MEASUREMENT USING UDEAS

Searching for optimal emission factors, which minimize error between measurements and model outputs, with conventional optimization algorithms is not an easy task. In this paper, a new optimization algorithm named uDEAS, which is effective and easily applicable, is employed to tune the 30 emission factors. At this step, the emission factors are tuned by using a multi-step tuning strategy.

4.1. uDEAS

Dynamic Encoding Algorithm for Searches (DEAS) has been developed as a new type of non-gradient optimization method [11,12]. The principle of DEAS is based on the distinct properties of binary strings. If a binary digit, 0 or 1, is appended to any binary string as a least significant bit (LSB), the decoded real number of a new binary string decreases for 0, and increases for 1 compared to that of the original binary string (i.e., bisectional search, BSS). Moreover, if a binary string undergoes an increment addition or a decrement subtraction, the real number of each processed string increases or decreases equidistantly (i.e., unidirectional search, UDS). These two characteristics of binary strings are adopted for the determination of search directions and step lengths in a local search phase. For a global search strategy, the multistart approach is embedded into DEAS with various revisit check functions for search efficiency. Details are found in a dedicated website 'www.deasgroup.net'. DEAS is now classified into two categories; exhaustive DEAS (eDEAS) and univariate DEAS (uDEAS). eDEAS is an original version of DEAS with the above-mentioned local search principles which suffer from exponential complexity as search dimension increases. uDEAS is designed especially for lightening the exponential computation burden in local search by modifying the philosophy of 'BSS for every parameter-UDS for every parameter' into the philosophy of 'BSS-UDS for each parameter in a sequential manner'. Owing to its simple structure, uDEAS requires no redundancy check routine [12] and its amount of cost evaluation for a single optimal transition is decreased from $O(2^n)$ to $O(2n)$. Effectiveness of uDEAS has been validated with the well-known benchmark functions whose landscapes are nonsmooth and/or highly multimodal. uDEAS is also being applied to an on-load parameter identification of induction motors for diagnosis with successful results.

4.2. Adaptation strategy

The emission factors are found by simulating the FEM model and comparing the simulation results with the measured billet temperatures for skid part. Using uDEAS, the emission factors are found by minimizing SSE (Sum Squared Error) between the model outputs and measurements. Let TC_i^{est} be a model output which is corresponding to the measured data of TC_i. The cost function with weighting factors, ρ_1, ρ_2, and ρ_3 is defined as follows:

$$\begin{aligned} Cost\ Function = & \sum_{CCR\ pattern} \rho_1 e_{top}^2 + \rho_2 e_{center}^2 + \rho_3 e_{bottom}^2 \\ & + \sum_{WCR\ pattern} \rho_1 e_{top}^2 + \rho_2 e_{center}^2 + \rho_3 e_{bottom}^2, \end{aligned} \quad (6)$$

where $e_{top} = (TC_{12}^{est} - TC_{12})$, $e_{center} = (TC_{13}^{est} - TC_{13})$, and $e_{bottom} = (TC_{14}^{est} - TC_{14})$. Define *Cost Function 1* and *Cost Function 2* by choosing $(\rho_1, \rho_2, \rho_3) = (100,1,100)$ and $(\rho_1, \rho_2, \rho_3) = (1,100,1)$, respectively. Since the temperatures of the skid parts are only measured along the billet thickness direction, it is natural to divide the tuning process into two stages:

Stage 1: Tune the $\varepsilon_{t1} \sim \varepsilon_{t10}$ and $\varepsilon_{b1} \sim \varepsilon_{b10}$ while the $\varepsilon_{s1} \sim \varepsilon_{s10}$ are being fixed.

Stage 2: Tune the $\varepsilon_{s1} \sim \varepsilon_{s10}$ while the $\varepsilon_{t1} \sim \varepsilon_{t10}$ and $\varepsilon_{b1} \sim \varepsilon_{b10}$ are being fixed.

Since only the conductive heat transfer occurs inside the billet as mentioned in the previous section, it is natural that e_{top} and e_{bottom} should be minimized with greater importance than e_{center}. At stage 1, since the measured data, TC_{12} and TC_{14}, are available along the billet thickness direction, *Cost Function 1* is chosen to give priority to e_{top} and e_{bottom}. At stage 2, *Cost Function 2* is chosen to give priority to e_{center} because the measured data such as TC_{12} and TC_{14} are not available along the billet width direction. If such measured data are available, the tuning process consists of just one stage and the emission factors can be obtained directly by using uDEAS. The above tuning process is carried out by using the following tuning strategy:

Step 1: Set the emission factors of the billet left/right sides as those of billet top side and then tune the emission factors of the billet top and bottom sides with *Cost Function 1*.

Step 2: Fix the emission factors of the billet top and bottom sides and then tune the emission factors of the billet left/right sides with *Cost Function 2*.

Step 3: Fix the emission factors of the billet left/right sides and then tune the emission factors of the billet top and bottom sides with *Cost Function 1*.

Step 4: Repeat step 2 once.

Since the above tuning process consists of multiple steps, the tuning results(i.e., the emission factors obtained by using uDEAS) are different at each step. It is observed that the tuning results vary within some bound as the tuning process is carried out (i.e., step 2 → step 3 → step 2 → step 3···). Hence, the tuning process is stopped after step 4 based on this observation.

4.3. Results

The emission factors, which are restricted from 0 to 1, are obtained by using the above scheme for the skid part as follows:

$$E \equiv \begin{bmatrix} \varepsilon_{t1} & \cdots & \varepsilon_{t5} \\ \varepsilon_{t6} & \cdots & \varepsilon_{t10} \\ \varepsilon_{b1} & \cdots & \varepsilon_{b5} \\ \varepsilon_{b6} & \cdots & \varepsilon_{b10} \\ \varepsilon_{s1} & \cdots & \varepsilon_{s5} \\ \varepsilon_{s6} & \cdots & \varepsilon_{s10} \end{bmatrix}, \quad (7)$$

$$E = \begin{bmatrix} 0.7143 & 0.7302 & 0.6032 & 0.6825 & 0.8254 \\ 0.3492 & 0.5714 & 0.4762 & 0.5556 & 0.5079 \\ 0.9048 & 0.6667 & 0.7619 & 0.6825 & 0.7460 \\ 0.3492 & 0.4444 & 0.4127 & 0.1270 & 0.1111 \\ 0.5397 & 0.7619 & 0.2698 & 0.0000 & 0.6349 \\ 0.0159 & 1.0000 & 1.0000 & 1.0000 & 1.0000 \end{bmatrix}.$$

The tuning results and corresponding errors are shown in Fig. 6. Let T_s and T_m represent the simulated and measured billet center temperature, respectively. Let e_{center} be an estimation error defined as $(T_s - T_m)$. Let e_{center_d} and $max|e_{center}|$ be an estimation error at discharging and corresponding maximum absolute estimation error, respectively. These e_{center_d} and $max|e_{center}|$ are shown in Table 1. Although the billet center temperatures at discharging after step 1 and 4 are similar, the corresponding maximum absolute errors during furnace operation are significantly reduced after step 4. It can be observed from Fig. 6 that the test billet shows a significant change in the specific heat at about $1040K$. However, the specific heat, which is adopted in this paper, shows a big change at about $1000K$. Therefore, even though an optimization algorithm is successfully applied to the tuning process, there always exists a maximum estimation error near this temperature range.

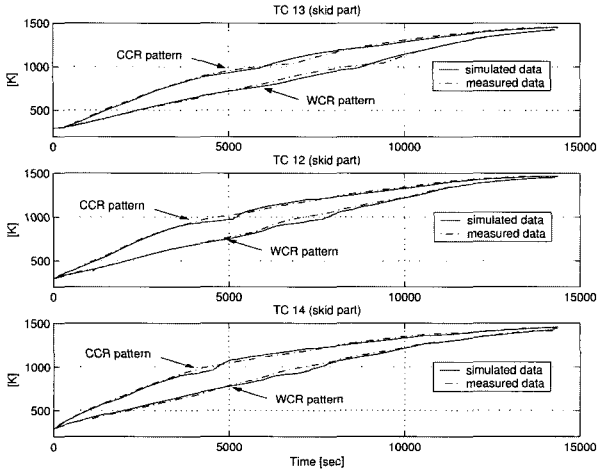

(a) Tuning results for the CCR/WCR pattern.

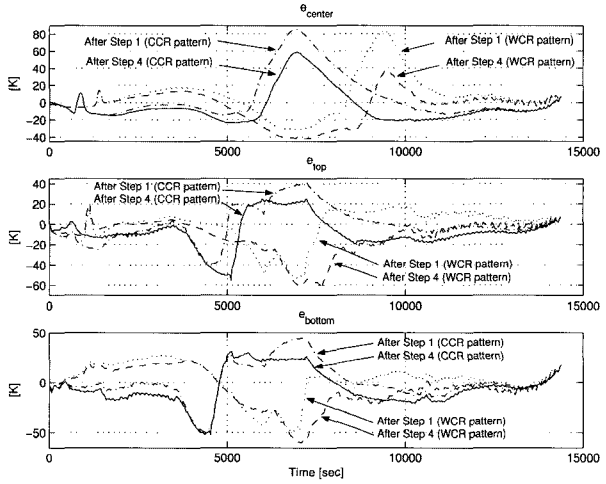

(b) Errors.

Fig. 6. Tuning results and its errors.

Table. 1. Estimation errors.

	CCR Pattern		WCR Pattern	
	e_{center_d}	$max \mid e_{center} \mid$	e_{center_d}	$max \mid e_{center} \mid$
step 1	6.3[K]	86[K]	3.2[K]	84.4[K]
step 4	7[K]	58.7[K]	4.6[K]	42[K]

4.4. Validation

In this section, the emission factors, which are obtained in the above section, are applied to a simulation for the other skid parts which are not used in the model tuning. TC_6 and TC_{17} are selected for this simulation. It is assumed that the ambient temperatures of the billet top side (i.e., TC_3, TC_{11}, and TC_{18}) are changed linearly. Hence T_{top} for TC_6 and TC_{17} are defined as $TC_{11} + (TC_3 - T_{11}) \times 2/3$ and $TC_{11} - (TC_{11} - T_{18}) \times 2/3$, respectively. The results are shown in Fig. 7. The estimation error at

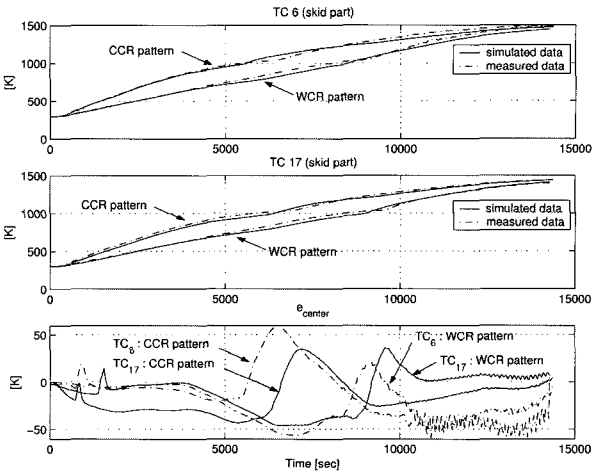

Fig. 7. Results for TC_6 and TC_{17}.

Table. 2. Estimation error for TC_6 and TC_{17}.

	CCR Pattern		WCR Pattern	
	e_{center_d}	$max \mid e_{center} \mid$	e_{center_d}	$max \mid e_{center} \mid$
TC_6	-4.1[K]	59.6[K]	8[K]	59[K]
TC_{17}	4.7[K]	43.3[K]	7.1[K]	46.2[K]

discharging, e_{center_d}, and corresponding maximum absolute error, $max \mid e_{center} \mid$, are shown in Table 2. It is observed that the results are acceptable.

5. CONCLUDING REMARKS

In this paper, a 2D billet heat transfer FEM model with spatially distributed emission factors is proposed to obtain an on-line information of billet temperatures during reheating furnace operation. At this step, the emission factors are assumed as a function of position and then are obtained by applying the proposed tuning strategy, which consists of 4 steps, with the aid of an optimization algorithm named uDEAS. The performance of the proposed model is shown by comparing the measured data with the corresponding model outputs.

REFERENCES

[1] *Technical Report of Combustion Control for a Reheating Furnace 2nd ed.*, POSCON, 1999.

[2] H. S. Ko, J.-S. Kim, T.-W. Yoon, M. K. Lim, D. R. Yang, and I. S. Jun, "Modeling and predictive control of a reheating furnace," *Proc. of American Control Conf.*, Chicago, Illinois, pp. 2725-2729, 2000.

[3] J. H. Choi, Y. J. Jang, and S. W. Kim, "Temperature control of a reheating furnace using feedback linearization and predictive control," *Proc. of International Conference on*

Control, Automation and Systems, Jeju, pp. 103-106, 2001.

[4] J. G. Kim and K. Y. Huh, "Prediction of transient slab temperature distribution in the re-heating furnace of a walking-beam type for rolling of steel slabs," *ISIJ International*, vol. 40, no. 11, pp. 1115-1123, 2000.

[5] *A Measurement of Heat Transfer in a Reheating Furnace and its Computation Method, a Subcommittee on Reheating Furnace*, The Iron and Steel Institute of Japan, 1971.

[6] L. M. Pedersen, *Modeling and Control of Plate Mill Processes*, Ph.D. thesis, Department of Automatic Control, Lund Institute of Technology, 1999.

[7] *FEMLAB Automatic Control Reference Manual*, COMSOL, 2000.

[8] Y. W. Kwon and H. C. Bang, *The Finite Element Method Using MATLAB 2nd ed.*, CRC Press, 2000.

[9] D. W. Pepper and J. C. Heinrich, *The Finite Element Method, Basic Concepts and Applications*, Hemisphere Pub. Corp., 1992.

[10] Y.-Y Yang and Y.-Z. Lu, "Development of a computer control model for slab reheating furnaces," *Computers in Industry*, vol. 7, no. 2, pp. 145-154, 1986.

[11] J.-W. Kim and S. W. Kim, "Numerical method for global optimization: Dynamic encoding algorithm for searches," *IEE Proc.-Control Theory Appl.*, vol. 151, no. 5, pp. 661-668, 2004.

[12] J.-W. Kim and S. W. Kim, "Parameter identification of induction motors using dynamic encoding algorithm for searches (DEAS)," *IEEE Trans. on Energy Conversion*, vol. 20, no. 1, pp. 16-24, 2005.

Yu Jin Jang received the B.S. degree from KAIST in 1996, and the M.S. and Ph.D. degrees from Pohang University of Science and Technology (POSTECH) in the area of automatic control in 1998 and 2002, respectively. He is currently an Assistant Professor of the Department of Information & Communication Engineering, Dongguk University, Kyungju, Korea. His research interests include system modeling, nonlinear control, and process automation.

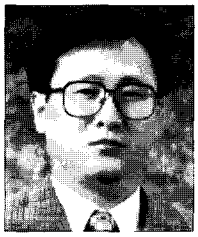

Sang Woo Kim received the B.S., M.S., and Ph.D. degrees from Department of Control and Instrumentation Engineering, Seoul National University, in 1983, 1985, and 1990, respectively. He is currently an Associate Professor in the Department of Electronics and Electrical Engineering at Pohang University of Science and Technology(POSTECH), Pohang, Korea. His current research interests are in optimal control, optimization algorithm, intelligent control, wireless communication, and process automation.